Electrochemical Modulation of the Photophysics of Surface-Localized Trap States in Core/Shell/(Shell) Quantum Dot Films

Van Der Stam, Ward; Grimaldi, Gianluca; Geuchies, Jaco J.; Gudjonsdottir, Solrun; Van Uffelen, Pieter T.; Van Overeem, Mandy; Brynjarsson, Baldur; Kirkwood, Nicholas; Houtepen, Arjan J.

DOI
10.1021/acs.chemmater.9b02908

Publication date
2019

Document Version
Final published version

Published in
Chemistry of Materials

CHEMISTRY OF MATERIALS
Cite This: Chem. Mater. 2019, 31, 8484−8493
Article
pubs.acs.org/cm

Electrochemical Modulation of the Photophysics of Surface-Localized Trap States in Core/Shell/(Shell) Quantum Dot Films

Ward van der Stam,*,† Gianluca Grimaldi, Jaco J. Geuchies, Solrun Gudjonsdottir, Pieter T. van Uffelen, Mandy van Overeem, Baldur Brynjarsson, Nicholas Kirkwood,‡ and Arjan J. Houtepen*

Opto-Electronic Materials Section, Faculty of Applied Sciences, Delft University of Technology, van der Maasweg 9, 2629 HZ Delft, The Netherlands

Supporting Information

ABSTRACT: In this work, we systematically study the spectroelectrochemical response of CdSe quantum dots (QDs), CdSe/CdS core/shell QDs with varying CdS shell thicknesses, and CdSe/CdS/ZnS core/shell/shell QDs in order to elucidate the influence of localized surface trap states on the optoelectronic properties. By correlating the differential absorbance and the photoluminescence upon electrochemically raising the Fermi level, we reveal that trap states near the conduction band (CB) edge give rise to nonradiative recombination pathways regardless of the CdS shell thickness, evidenced by quenching of the photoluminescence before the CB edge is populated with electrons. This points in the direction of shallow trap states localized on the CdS shell surface that give rise to nonradiative recombination pathways. We suggest that these shallow trap states reduce the quantum yield because of enhanced hole trapping when the Fermi level is raised electrochemically. We show that these shallow trap states are removed when additional wide band gap ZnS shells are grown around the CdSe/CdS core/shell QDs.

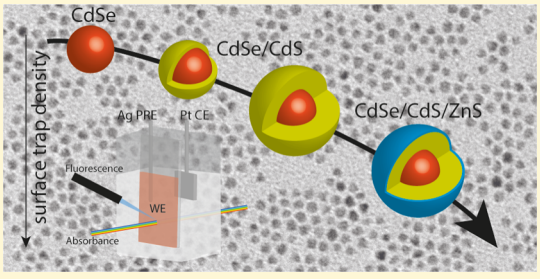

INTRODUCTION

The possibility to combine multiple semiconductor materials into one nanocrystal has opened up a variety of design strategies for colloidal nanomaterials.[1−9] A judicious choice of the size and shape of the two components not only leads to tunability of the emission wavelength but can also result in spatial charge carrier separation,[1,3,10] prolonged exciton lifetimes,[1,11] suppressed Auger recombination (AR),[12−15] and enhancement of the photoluminescence quantum yield (PLQY).[12,16−18] The PLQY of semiconductor core/shell QDs upon epitaxial shell overgrowth mainly increases due to the reduced number of surface trap states on the core material,[16,18−20] which enhances the radiative band-edge recombination with respect to the nonradiative recombination pathways via trap states within the band gap. Elucidating the contribution of these localized surface trap states to the optoelectronic properties, and subsequent removal of these trap states, is thus of high interest for the community working on colloidal nanomaterials.

The combination of a CdSe core and CdS shells is heavily studied because of their near-unity PLQY values.[16−18,21,22] According to the bulk energy levels, the combination of CdSe and CdS in one material should result in a type-I band alignment,[1] in which the exciton is confined to the CdSe core and the CdS shell acts as an antenna to increase the absorbance of high energy photons, which are subsequently funneled to the emissive CdSe core. These characteristics make CdSe/CdS quantum dots (QDs) very promising as color converters in television screens and for use as light-emitting diodes and QD lasers.[23−28] Despite their technological importance, many properties of CdSe/CdS core/shell QDs remain poorly understood. For instance, even in very thick-shelled CdSe/CdS QDs, the presence or absence of specific surface ligands affects the PLQY, suggesting that photogenerated charge carriers still have access to the surface,[18,21] where they are trapped on unknown in-gap states.[29] Other evidence for the existence of trap states in core/shell CdSe/CdS QDs comes from significant delayed photoluminescence (PL), associated with temporary charge carrier trapping at the interface or QD shell surface.[11] However, a direct measurement of such shell-localized surface trap states has so far remained elusive.

In this work, we systematically study these localized surface trap states in CdSe QDs, CdSe/CdS core/shell QDs with varying shell thicknesses, and CdSe/CdS/ZnS core/shell/shell QDs by correlating in situ absorbance and PL spectroelectrochemistry (SEC) measurements. We reveal that trap states near the conduction band (CB) edge are present in CdSe and CdSe/CdS QDs, evidenced by PL quenching before electrochemical population of the CB edge states occurs. We suggest that these shallow trap states result in rapid hole trapping when

Received: July 22, 2019
Revised: September 23, 2019
Published: September 24, 2019

DOI: 10.1021/acs.chemmater.9b02908
Chem. Mater. 2019, 31, 8484−8493

they are filled with electrons upon raising the Fermi level by applying an external potential.

The (spectro)electrochemical methods deployed in our work bear similarities with previous (spectro)electrochemical studies on core/shell QDs,[30,31] but the presence of shallow trap states, as suggested in our work, was not observed previously. We hypothesize that such shallow trap states were potentially masked in the previous literature because of differences in the way the electrochemical experiments were performed. One notable difference is the lower onset potential for charging, likely due to the larger QD size that was used in ref 30.

Interestingly, we observe that the shallow traps are no longer present when additional wide band gap ZnS shells are grown on the CdSe/CdS QDs, suggesting that the trap states are related to the presence of Cd on the surface. We hypothesize that the traps responsible for this are undercoordinated Cd atoms that form Cd−Cd dimers at the CdS surface, in accordance with the recent theoretical work from our group.[32] Our work elucidates the effect of surface-localized traps on the optoelectronic properties of core/shell/(shell) QDs and shows that charge injection by electrochemistry is a powerful method to tailor, study, and understand these properties.

METHODS

Materials. Cd(II) acetate ($CdAc_2$, 98%), zinc acetate ($ZnAc_2$, 99.999%), selenium powder (Se, 99.999%), trioctylphosphine oxide (TOPO, 90%), trioctylphosphine (TOP, 97%), 1-octadecene (ODE, 90%), octadecylamine (ODA, 90%), sulfur powder (S, 99.98%), oleic acid (OA, 90%), oleylamine (OLAM, 70%), 1-octanethiol (98.5%) 1,7-diaminoheptane (7DA, 98%), 1,8-octanedithiol (8DT, 97%), lithium perchlorate ($LiClO_4$, 99.99%), ferrocene (Fc, 98%), and anhydrous solvents (toluene, 99.8%, methanol, MeOH, 99.8%, 1-butanol, BuOH, 99.9%, acetonitrile, 99.99%) were all purchased from Sigma-Aldrich and used as received, except for the acetonitrile, which was dried before use in an Innovative Technology PureSolv Micro column. The indium-doped tin oxide (ITO) substrates (film thickness 100 μm, $R_{sq} \leq 120\ \Omega/cm^2$) were purchased from PGO Germany and used as received.

Synthesis of CdSe Core QDs. The colloidal CdSe core QDs were synthesized following the hot injection method presented by Qu et al.[33] For the synthesis, Cd and Se precursors were prepared. The Cd precursor was prepared by degassing 1.32 g of $CdAc_2$, 7.41 g of OA, and 52.4 g of ODE for 3 h at 120 °C. The Se precursor was prepared by dissolving 1.42 g of Se powder in 7.50 g of TOP and 11.9 g of ODE at 200 °C. For the synthesis of ∼3.5 nm CdSe core NCs, 1.11 g of TOPO, 3.2 of ODA, and 5.2 g Se precursor were loaded in a 25 mL three-neck flask and degassed for 1 h at 120 °C, after which the flask was purged with N_2. Under the N_2 atmosphere, the solution was heated to 300 °C, after which 4.9 g of the Cd precursor was rapidly injected. The temperature was kept at 280 °C for 9 min, after which the flask was cooled with an air gun. When the temperature dropped below 100 °C, 6 mL anhydrous toluene was added to quench the solution. The QDs were precipitated by the addition of one equivalent of methanol and butanol and centrifugation for 5 min at 3500 rpm and redispersed in ∼6 mL toluene. This washing step was repeated once more.

Synthesis of CdSe/CdS Core/shell QDs (Procedure A). The CdSe/CdS QDs were synthesized using the successive ion layer addition reaction method.[34] First, 100 nmol of the synthesized CdSe QDs were dispersed in 2 mL OLAM and 4 mL ODE in a three-neck flask. The concentration of the QD dispersion was determined using an extinction coefficient of 223 181 $M^{-1}\ cm^{-1}$.[35] Then, the solution was degassed for 1 h at 120 °C. The S-precursor was prepared by dissolving 1.6 g of sulfur in 50 mL ODE at 200 °C. The same Cd precursor solution as described above was used for the CdS shell growth. The CdSe core QD solution was heated to 240 °C under the N_2 atmosphere and the Cd and S precursors were injected using a syringe pump for gradual addition. The addition rate was one shell per hour, in which a shell is defined as one atomic layer of CdS. Afterward, the solution was cooled down to 100 °C with an air gun and quenched with 6 mL toluene. Subsequently, the QDs were precipitated by the addition of one equivalent MeOH and BuOH and centrifugation for 5 min at 3500 rpm. Finally, the CdSe/CdS core/shell QDs were redispersed in ∼2 mL of toluene. This washing step was repeated once more.

Synthesis of CdSe/*x*CdS QDs (Procedure B) and CdSe/CdS/ZnS Core/Shell/Shell QDs. The core/shell/shell QDs were synthesized by adding Zn-oleate and octanethiol in ODE with syringe pumps at 230 °C, according to the procedure published by Boldt et al.,[36] to CdSe/CdS QDs prepared according to the protocol described by Chen et al. (procedure B).[8] During the addition of the Zn and S precursors, the temperature was allowed to gradually increase to 310 °C.[36] The Zn-oleate precursor solution was prepared by dissolving 367 mg of $ZnAc_2$ in OA (1.13 g) and ODE (7.0 mL) at 200 °C until a clear solution is obtained, after which it is cooled to room temperature.[65]

QD Film Preparation. The QD films were prepared in a N_2 purged glovebox using a dip coater from Nima Technology. ITO-covered glass plates were consecutively dipped for 30 s in a concentrated colloidal dispersion of QDs, a 14 v % solution of 8DT or 7DA ligands in methanol to cross-link the QDs, and a methanol solution in order to remove the excess, unbound ligands. The abovementioned procedure was repeated 10 times in order to obtain sufficiently thick QD films (∼100−200 nm). Afterward, the plates were dried for an hour inside the glovebox. Roughly, a third of the ITO substrates were left uncoated to ensure contact for the electrochemistry measurements discussed below. The QD films on ITO were used as the working electrode (WE) in the spectroelectrochemical measurements described below.

(Spectro)electrochemistry. The (spectro)electrochemical experiments were performed in a three-electrode electrochemical cell, consisting of a Ag wire pseudoreference electrode (PRE), a platinum (Pt) plate counter electrode, and the abovementioned QD-ITO WE. All experiments were performed inside a N_2 purged glovebox. The supporting electrolyte was 0.1 M $LiClO_4$ in acetonitrile solution. A PGSTAT128N Autolab potentiostat was used to regulate the potential and measure the current. A schematic of the electrochemical cell can be found in Supporting Information, Figure S20. Cyclic voltammograms were recorded with a scan speed of 0.03 V/s (CdSe and CdSe/*x*CdS QDs) or 0.02 V/s (CdSe/*x*CdS/ZnS QDs). The Ag-wire PRE was calibrated with a ferrocene/ferrocenium redox couple between applied potentials of −1.0 and +1.5 V at a scan rate of 0.05 V/s (Ag PRE vs vacuum: 4.92 V, Supporting Information, Figure S5).[37,38] During electrochemical charging, differential absorbance spectra were recorded on a USB2000+ spectrometer (Ocean Optics, range 200−1025 nm) and detected with optical fibers. The white light source was a DH-2000 deuterium halogen UV−VIS−NIR lightsource from Ocean Optics. A background correction was made with a blank ITO plate prior to measurements. A schematic of the setup can be found in Supporting Information, Figure S21.

In Situ PL SEC. The same electrochemical cell and detector as described above were used for the in situ PL experiments. The sample was excited with a 405 nm Thorlabs laser under a 45° angle and focused onto the sample with a lens. The PL was detected perpendicular to the sample, and the PL was focused onto the detection fiber by two lenses. A schematic of the setup can be found in Supporting Information, Figure S21.

Ex Situ Optical Spectroscopy. Ex situ optical measurements were performed on diluted colloidal dispersions in toluene. Samples were prepared by diluting the stock solution of washed QDs with anhydrous toluene under nitrogen, and samples were stored in closed quartz cuvettes (optical path length 1 cm). Absorbance spectra were measured on a double-beam PerkinElmer Lambda 900 UV/vis spectrometer. PL spectra were recorded on an Edinburgh Instruments FLS980 spectrofluorimeter equipped with a 450 W Xenon lamp as the excitation source and double grating monochromators. PLQY values

DOI: 10.1021/acs.chemmater.9b02908
Chem. Mater. 2019, 31, 8484−8493

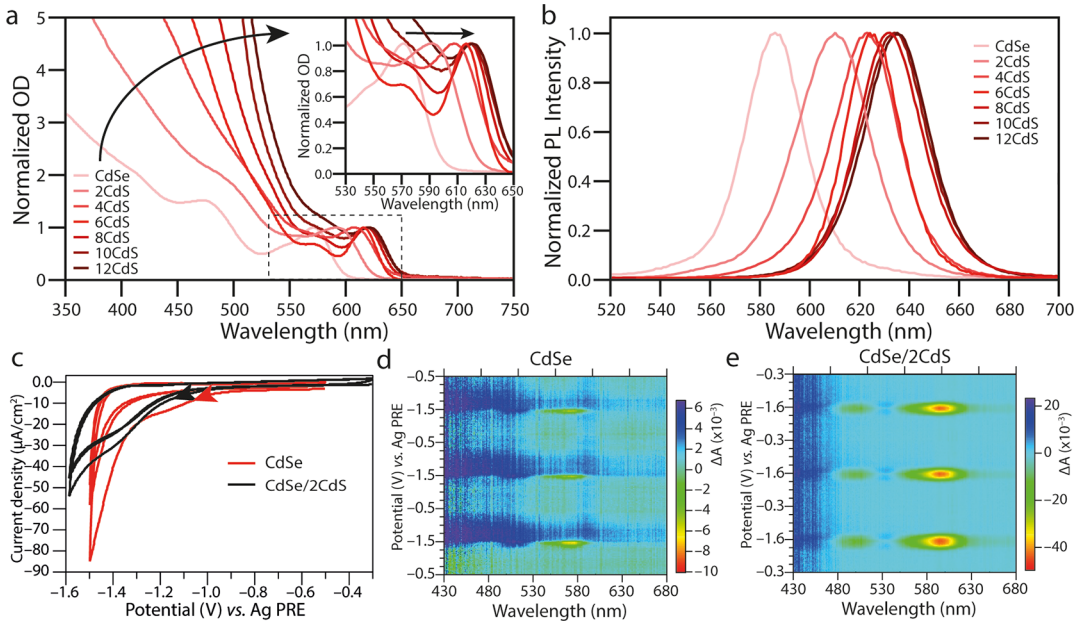

Figure 1. Characterization of CdSe and CdSe/*x*CdS core/shell QDs. (a) Absorbance spectra of CdSe and CdSe/*x*CdS core/shell QDs, revealing an increase in absorbance below 500 nm for increasing CdS shell thickness and a red shift of the band-edge transition (inset). (b) PL spectra of CdSe and CdSe/*x*CdS QDs, showing a red shift of the PL maximum upon increasing shell thickness. (c) Cyclic voltammograms of a CdSe QD film (red line) and a CdSe/2CdS QD film (black line) on ITO in 0.1 M $LiClO_4$ in the acetonitrile supporting electrolyte with a scan rate of 30 mV/s. (d) Differential absorbance as a function of the applied potential for CdSe core-only QDs and (e) for CdSe/2CdS core/shell QDs. The band-edge bleach around 580 nm becomes more reversible upon epitaxial CdS shell overgrowth.

were obtained with respect to a reference dye (rhodamine 6G in ethanol, PLQY 96%).

Transmission Electron Microscopy and Electron Diffraction. TEM samples were prepared by drop-casting dilute solutions of QDs in toluene on carbon-coated copper TEM grids (400-mesh). TEM images and electron diffraction patterns were measured on a JEOL JEM-1400 TEM, operating at 120 kV.

RESULTS AND DISCUSSION

Synthesis and Characterization of CdSe and CdSe/CdS QDs. CdSe, CdSe/CdS core/shell, and CdSe/CdS/ZnS core/shell/shell QDs were synthesized according to existing literature protocols.[8,33,34] Characterization with transmission electron microscopy (TEM) showed an increase in particle size for an increasing number of CdS shells (Supporting Information, Figures S1 and S2 and Table S1) and ZnS shells (Figures S3 and S4), which closely matches the calculated number of CdS shells based on the final QD size (Supporting Information, Table S1), taking the zinc blende CdS lattice parameter into account. Optical spectroscopy revealed a red shift of the band edge transition upon increasing CdS shell thickness (Figure 1a), as well as a red shift of the PL maximum (Figure 1b). Furthermore, thick CdS shells result in a sharp increase in absorbance below 500 nm, corresponding to absorbance from the CdS shell (Figure 1a). The PLQY was measured for all core/shell and core/shell/shell samples, and values ranging from 10 to 50% were found for CdSe/CdS QDs and values around 80% for CdSe/CdS/ZnS QDs (Supporting Information, Table S2). In total, nine samples were prepared: CdSe core QDs, six CdSe/*x*CdS core/shell QDs (with x = 2, 4, 6, 8, 10, and 12) and two CdSe/*x*CdS/ZnS core/shell/shell QDs (with x = 2 and 6). All measurements and analyses discussed in this paper were conducted on all samples, and the results can either be found in the main text or in the Supporting Information.

In Situ Absorbance and PL SEC. SEC is a useful method to study charge carrier recombination phenomena in films of colloidal QDs because the application of an electrochemical potential controls the Fermi level, which results in controlled charge injection into the QDs.[30,37,39−43] This charge injection can result in trap state filling/emptying and/or band-edge population, which have distinct influences on the optoelectronic properties of the QDs.[42,44−46] By precisely correlating absorbance and PL SEC, we can disentangle the effects of band filling and trap filling.[42,44−47]

Because the band edge absorbance (corresponding to the $1S_{3/2}1S_e$ transition for Cd-chalcogenide QDs) scales with the number of electrons in the $1S_e$ electronic state via $\langle N_e \rangle = g\Delta A/A_0$ (where $\langle N_e \rangle$ is the average number of electrons in a particular electronic state, ΔA is the differential absorbance, A_0 is the steady state absorbance, and g is the degeneracy of the electronic state, which is 2 for the $1S_e$ CB level of Cd chalcogenides),[30] measuring the differential absorbance during cyclic voltammetry (CV) measurements allows us to determine the average number of electrons in the CdSe CB as a function of the applied potential. CV (Figure 1c) and differential absorbance measurements (Figure 1d,e) indicated charge injection at potentials of <−1.0 V versus the Ag PRE (which we estimate to lie at 4.92 V vs vacuum, Figure S5)[48] for both CdSe and CdSe/2CdS QDs, with $\langle N_{1S_e} \rangle$ = 0.2 and 1.7, respectively.

From the combination of these differential absorbance plots and CV measurements, it is evident that the epitaxial growth of a thin CdS shell on the CdSe core not only has a dramatic impact on the reversibility of the charge injection but also on the average number of electrons in the CB edge (0.2 for CdSe vs 1.7 for CdSe/2CdS, Supporting Information, Figures S6 and S7). We consider that the maximum number of electrons per QD reflects a steady-state population, where electrochemical

DOI: 10.1021/acs.chemmater.9b02908
Chem. Mater. 2019, 31, 8484−8493

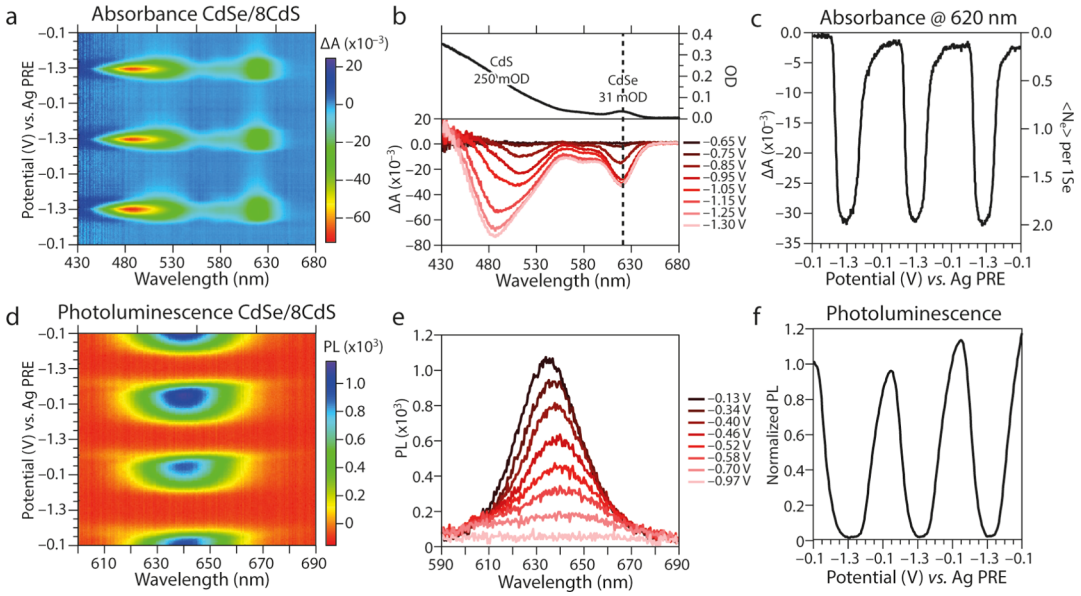

Figure 2. Example of in situ SEC measurements on CdSe/CdS core/shell QDs. (a) 2D differential absorbance plot of CdSe/8CdS QDs upon applying a potential, showing negative absorbance features around 620 and 490 nm at the maximum applied potential, corresponding to the CB edge of the CdSe core (620 nm) and the first exciton transition of the CdS shell (490 nm). (b) 1D differential absorbance (ΔA) plots at different applied potentials and the steady-state absorbance (top, black line, A_0). The dashed line gives the position at which the intensity versus potential trace (panel c) was recorded. (c) Differential absorbance as a function of applied potential (left axis), which linearly scales with the average number of electrons in the CB edge (right axis). A maximum of 2 electrons are injected into the CdSe band edge. (d) 2D PL SEC as a function of applied potential, showing quenching of the PL upon charge injection. The PL is fully recovered when the scan is reversed. (e) 1D PL spectra at different applied potentials, showing quenching and a small red shift of the maximum at more negative applied potentials. The full PL peak was integrated, in order to follow the (f) PL intensity as a function of applied potential.

electron injection is balanced by loss of electrons to reduction of solvent impurities and surface trapping. The higher $1S_e$ charge density in core/shell QDs thus suggests a reduced amount of surface trapping, in line with the higher PLQY for these samples (Supporting Information, Table S2). For core/shell QD films, we observe the absorption bleach of CdS localized transitions at shorter wavelengths (around 480 nm). This becomes especially pronounced for thicker CdS shells as shown for instance in Figure 2a,b for CdSe/8CdS. The bleach of the CdS shell absorption appears at somewhat more negative potentials than the bleach of CdSe core transitions. As discussed in the Supporting Information, Figure S8 and associated text, this suggests a small type I band offset of ∼0.3 V between the CdSe and CdS conduction levels, regardless of the CdS shell thickness.

To investigate the influence of traps on the PL, we performed in situ PL SEC and absorbance SEC simultaneously and compared the potential dependence of the radiative recombination to the potential dependence of the differential absorbance measurements (Figure 2). Because the PL of QDs is very sensitive toward nonradiative recombination via trap states, this combination of techniques allows us to distinguish between nonradiative recombination pathways due to band-edge population (showing a decrease of both absorbance and PL) and trap states (showing a decrease of PL only).

Figure 2 shows a typical in situ absorbance and PL SEC experiment on a film of CdSe/CdS core/shell QDs (in this case, CdSe/8CdS). The differential absorbance as a function of the applied potential is very reversible (Figure 2a). From the absorption difference spectra (Figure 2b), we can deduce that the average number of electrons in the $1S_e$ CB edge electronic state ($\langle N_{1S_e} \rangle$) is ∼2 at the maximum applied potential (−1.3 V vs Ag PRE, Figure 2c). Furthermore, we also see bleaching of $1P_e$ associated transitions in the differential absorbance spectra (evidenced by the continued bleaching of the transition at 580 nm after the $1S_{3/2}-1S_e$ transition has saturated, Figure 2b), showing that the total number of CB electrons per QD exceeds 2.

In situ PL SEC (Figure 2d,e) reveals the influence of additional charge carriers on the radiative recombination.[40,49] The PL is spectrally integrated (Figure 2e) and shown as a function of potential in Figure 2f. We find that the PL changes become more reversible upon the growth of epitaxial CdS shells (Figure 2f), when compared to core-only CdSe QDs (Figure 3a). The same experiments were performed for all CdSe/xCdS nanocrystals, which showed similar trends in terms of the reversibility of the PL (Supporting Information, Figures S9−S14).

Figure 3 compares the differential absorbance and PL intensity as a function of the applied potential for CdSe and CdSe/xCdS QDs with different shell thicknesses (indicated by x). This analysis reveals that the PL drops before the CdSe CB edge is reached (i.e., before there is an observable absorption bleach) for core-only CdSe QDs (Figure 3b) and CdSe/CdS core/shell QDs (Figure 3d,f). Importantly, the decrease in PL intensity for core/shell QDs is found to be reversible because we always observe that the PL returns to its original intensity within several minutes when the potential is moved back to the open-circuit value. Hence, the offset between the onset of PL quenching and band-edge bleach is attributed to charge injection into trap states near the CB edge and not to irreversible cathodic decomposition of the QDs, as will be discussed in more detail below.

We have also performed kinetic measurements, recording the absorption and PL versus time upon a step in potential.

DOI: 10.1021/acs.chemmater.9b02908
Chem. Mater. 2019, 31, 8484−8493

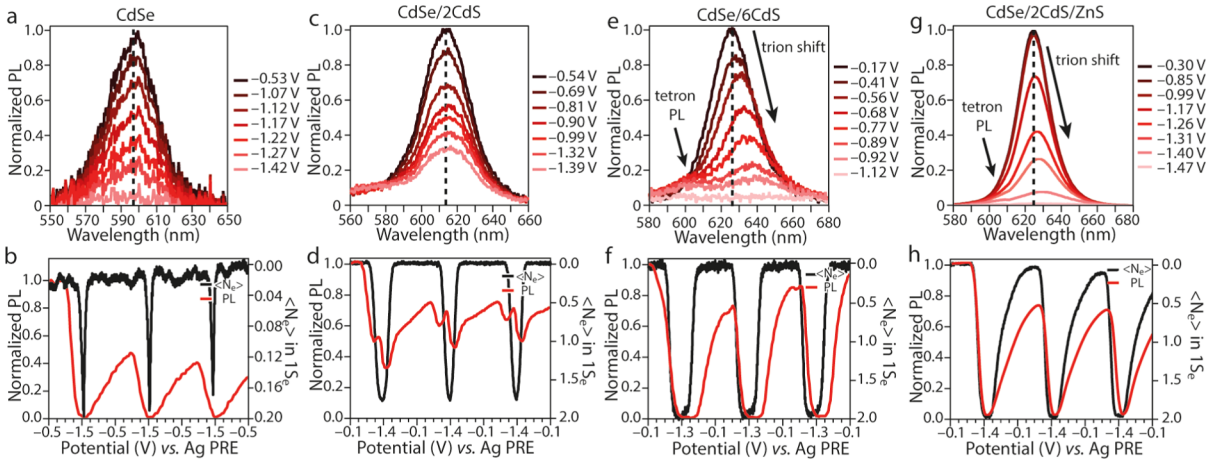

Figure 3. Comparison of differential absorbance and PL upon applying a potential. 1D PL traces at different potentials (a,c,e,g) and differential absorbance/average number of electrons in the CB edge vs PL intensity at different applied potentials plots (b,d,f,h) for (a,b) CdSe, (c,d) CdSe/2CdS, (e,f) CdSe/6CdS, and (g,h) CdSe/2CdS/ZnS QDs, showing tetron PL involving P-state electrons for thicker CdS shells and core/shell/shell QDs. PL quenching before CB state filling due to trap-assisted AR is observed for CdSe and CdSe/CdS core/shell QDs (b,d,f). This offset between absorbance bleach and PL quench is not present for CdSe/2CdS/ZnS core/shell/shell QDs (h).

When the potential is stepped from the open-circuit potential to −0.85 V, which corresponds to a Fermi level below the CB, we observe a very strong drop in PL, even when no change in absorption is observed (Figure S15 in the Supporting Information). When the potential is stepped to −1.5 V (within the CB), both the PL and absorption decrease, and strong hysteresis between the forward step to −1.5 V and the step back to the open-circuit potential is observed (Figure S15, Supporting Information). The hysteresis for the absorption bleach and PL quenching is very different and even opposite: the 1S absorption recovers more quickly upon the step back, the PL quenches more quickly upon the forward step.

This hysteresis can be explained by trap filling/emptying. Because electron transport probably only takes place between delocalized CB levels, electrons in localized trap states need to be thermally promoted to the CB to diffuse through the QD film.[50] The activation energy involved is the separation between the Fermi level and the CB energy level. Thus trap filling/emptying is relatively fast when the Fermi level is close to the CB but slow when the Fermi level is deep inside the band gap. In CV or CA measurement, in the reverse (anodic) scan or step, electrons are quickly removed from the 1S levels, but some electrons remain in deep traps causing the PL to recover much more slowly than the absorption.

Our results in Figure 3 show that for all CdS shell thicknesses, there is an offset between PL quench and band-edge bleach. The exact onset and the amount of hysteresis in the PL potential dependence varies for different shell thicknesses. This indicates that the number of shallow trap states is different in each sample.

The observation of trap filling and its effect on the PL intensity is in contrast with observations presented by Jha and Guyot-Sionnest.[30] By performing spectroelectrochemical measurements, they observed that the PL and the band-edge absorption starts to decrease at the same potentials and with the same kinetics, while we observe a clear drop in PL intensity before the onset of absorption bleaching. This could point to differences in the exact surface chemistry between our samples and the samples investigated in ref 30. However, given the ∼2% PLQY in the thin-film samples in ref 30 (which is similar to the PLQY of the films in this work) and given the fact that neutral QDs showed deep trap PL that disappeared upon electron charging in ref 30; numerous electrochemically active traps were clearly present in both this work and in ref 30. It is conceivable that the relatively small offset between the change in PL intensity and the absorption bleach was missed in the experiments shown in ref 30, given the higher scan rate and lower potential resolution of the optical data presented. Alternatively, the differences could point to the presence of different types of surface traps and corresponding different photophysical responses upon filling of these traps. This reinforces the need for systematic investigation of the nature and energy distribution of traps on QD surfaces.

We observe here that the PL efficiency *reduces* when the Fermi level is raised near the CB (Figure 3 and Supporting Information, Figures S9−S14). In contrast, for CdTe QDs, we have observed an *increase* in PLQY upon raising the Fermi level within the band gap.[44,50] In the case of CdTe QDs, we found that the Fermi level at the open-circuit potential lies within a distribution of trap states near the valence band (VB),[44,50] whereas in the case of CdSe and CdSe/CdS core/shell QDs discussed here, we propose that the trap states lie above the Fermi level at the open-circuit potential, close to the CB (Figure 4a). Filling these shallow trap states with electrons will lead to decreased electron trapping and increased hole trapping. The fact that the PL decreases shows that the latter effect is dominant, which means that the hole capture rate constant is higher than the electron capture rate constant.[44]

For holes to get trapped nonradiatively in states close to the CB, much more energy needs to be dissipated than for electrons to get trapped at the same states. The fact that under these conditions hole trapping (when the states are full) is faster than electron trapping (when the states are empty) is unexpected if the trapping event is mediated by phonon emission. Therefore, we suggest that the hole trapping process is Auger-assisted and involves excitation of the photogenerated electron from the CB edge to higher energy (see schematic in Figure 4b). Auger-assisted trapping has been suggested before by Frantsuzov and Marcus[51] and has been described theoretically in detail by Califano et al.[52] We have also argued before that Auger-assisted trapping is responsible for fast *electron* trapping at states near the VB in CdTe QDs.[44]

DOI: 10.1021/acs.chemmater.9b02908
Chem. Mater. 2019, 31, 8484−8493

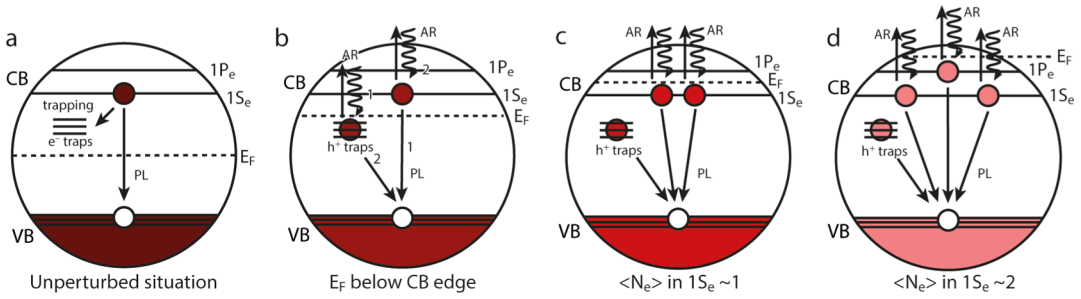

Figure 4. Mechanisms for radiative and nonradiative recombination pathways in electrochemically doped CdSe/CdS QDs. (a–d) Schematics showing the different processes that occur after photoexcitation when the Fermi level (E_F) is (a) in the middle of the band gap, (b) just above the trap states in the band gap, (c) above the $1S_e$ CB edge, and (d) above the $1P_e$ CB state. (a) After photoexcitation, the photogenerated electron can get trapped in states within the band gap, hence contributing to nonradiative recombination or recombine radiatively with the hole in the VB. (b) When the Fermi level is just above the distribution of shallow trap states, an electron in a trap state can get excited to higher energy states within the CB band when the electron and hole recombine, without emitting a photon, through trap-assisted AR (pathway 1), or the photogenerated hole can get trapped on the in-gap state, which promotes the photogenerated electron higher up in the CB through AR (pathway 2). (c) A negative trion and (d) a negative tetron result in additional radiative and nonradiative recombination pathways, which outcompete each other depending on the number of electrons per nanocrystal.

For CdSe core-only QDs (Figure 3a,b), when the Fermi level is raised further and the CB edge is reached, efficient nonradiative AR of negative trions occurs between electrochemically injected electrons in the CB and the photogenerated exciton, which entirely quenches the PL (Figure 4c). Upon reversing the applied potential, electrons are quickly withdrawn from the CB edge, but trap states are less readily emptied,[50] resulting in hysteresis in the PL trace (Figures 3b and S16). Furthermore, for core-only CdSe QDs, the PL decrease is only partially reversible, and some of the PL never recovers on the timescale of our experiments (Figure 3a). This hints to irreversible cathodic decomposition reactions. Our observations point toward a strong reduction of surface traps upon shell growth. However, we note that unity PLQY values are not reached for core/shell CdSe/CdS (Table S2), regardless of the shell thickness, suggesting that there are still nonradiative pathways, possibly associated with interfacial or shell-surface traps,[18] that give rise to a decrease in PL intensity when the Fermi level is raised. The elimination of core surface trap states likely also increases the electrochemical stability of the NCs because of a reduction of electrochemical side reactions at the NC surface. These side reactions can be generally described as $Cd^{2+} + 2e^- \rightarrow Cd^0$. The standard reduction potential of this reaction will depend on the coordination of the Cd^{2+} ion on the QD surface. Undercoordinated surface Cd^{2+} cations are a typical source of electronic traps,[20,53] and they are also the most vulnerable sites for cathodic decomposition. Hence, the removal of core surface electron traps by epitaxial shell growth will result in both an improved PLQY and an improved electrochemical stability.

Our results, as well as the results presented in ref 30, show that the CdS surface is less prone to electrochemical side reactions than the CdSe surface. This observation is somewhat surprising as the cathodic decomposition of CdS is usually found to occur at less negative potentials than the decomposition of CdSe.[54,55] Perhaps the reduced accessibility of the electron at the surface of CdSe/CdS QDs due to the Type-I band offset (Figure S8) may explain the enhanced stability because the electron predominantly resides in the CdSe core.

We further analyzed the PL dependence on the applied potential for the CdSe/*x*CdS QDs of different CdS shell thicknesses (Figure 3c–f). Similar to what was described above for the CdSe core-only QDs, a drop in PL intensity is observed before the onset of absorption bleach, indicating that hole trapping also occurs in CdSe/CdS core/shell QDs (see Figures 3d,f and 4b).[56–58] We find that this is the case for *all* shell thicknesses (Figures 3d,f and S9–S14, Supporting Information) and even for different synthesis protocols for the CdSe/*x*CdS QDs (Figure S17). Apparently, the growth of CdS shells does not eliminate all shallow traps below the CB. We suggest that these are surface traps on the CdS shell, probably associated with undercoordinated Cd surface atoms.

As discussed above, the fact that the PL *decreases* upon raising the Fermi level shows that the trapping rate constant is higher for holes than for electrons. This shows, surprisingly, that holes still interact with these surface traps, even in the case of thick CdS shells. In native QDs without an external applied potential, the Fermi level lies near the middle of the band gap and these traps are empty. In that case, hole trapping will not be dominant and the PLQY can be high, as is often observed for such core/shell QDs.[1,18,59]

We find that the offset between PL quenching and the $1S_{3/2}1S_e$ absorption bleach is removed upon the growth of a thin ZnS epitaxial shell on CdSe/2CdS and CdSe/6CdS QDs (Figure 3g,h and Supporting Information, Figure S18). These samples have high PLQY values of ~85% in solution and ~62% in a film (vs ~2% PLQY for the CdSe/*x*CdS films). With such a high PLQY for the investigated films, it is to be expected that most traps have been removed. The correlation between in situ absorbance and PL SEC uniquely allows for direct determination of the removal of shallow trap states. As shown in Figure 3h, for these ZnS-coated core/shell/shell QDs, we find that the PL quenches and the $1S_{3/2}1S_e$ absorption starts to bleach at exactly the same potential. Thus, there is no effect of changing the Fermi level on the PL efficiency, as long as the Fermi level is in the band gap.

These results show that there is a correlation between PLQY and the density of shallow trap states near the CB edge for Cd-chalcogenide QDs. Furthermore, passivation of CdSe cores with CdS shells is not sufficient to eliminate all of these shallow trap states, while subsequent overgrowth with ZnS does eliminate these traps. We speculate that the surface traps observed here are caused by undercoordinated Cd atoms at the surface of the CdSe core and/or the CdS shell. According to

DOI: 10.1021/acs.chemmater.9b02908
Chem. Mater. 2019, 31, 8484–8493

previous density functional theory (DFT) calculations, orbitals on undercoordinated Cd atoms do not have energies in the band gap and should therefore not act as traps.[20] However, more dynamic surface structures could possibly be responsible for traps near the CB that originate on Cd. One example that we consider is that Cd−Cd dimers might form on the surface (similar to what has been proposed for Pb−Pb dimers in PbS)[60] and that the bonding orbital of these dimers could result in states within the band gap. We recently studied the formation of such Cd−Cd dimers with DFT calculations which include n-doping and concomitant surface restructuring of the QDs.[32] Recently, epitaxial QD dimers were proposed as possible trap states in QD films.[61] We hypothesize that the formation of states in the band gap due to epitaxial QD dimers, or larger aggregates, may also occur for our CdSe-based core/shell QDs. However, occupation of such epitaxial QD dimer states by electrons would not quench the PL of the entire film, only the PL of the few dimers/aggregates involved, and hence we find it unlikely that such states are responsible for the observed electrochemical modulation of the PL. For the CdSe/CdS/ZnS core/shell/shell QDs, the undercoordinated cations on the surface will be Zn, rather than Cd, and their energy levels will likely be higher in energy, above the CB. Indeed, the standard reduction potential of Zn^{2+} is 0.36 V more negative than of Cd^{2+},[62] and our recent DFT calculation shows an improved electrochemical stability of ZnS surfaces compared to CdSe and CdS surfaces.[32]

For all shell thicknesses, we find that at the most negative potentials, the PL intensity drops strongly because of efficient AR between photogenerated excitons and electrochemically injected electrons (i.e. negative trions, Figure 4c). However, for thin CdS shells we observe that the PL intensity first *increases* when electrons are injected into the $1S_e$ levels (Figure 3d). Similar complicated PL dependences, but as a function of time after a potential step instead of as a function of potential in a CV, have been reported by Guyot-Sionnest et al.[63] and by Mulvaney et al.[31] We suggest that this behavior may be caused by the competition between radiative recombination, AR, and charge trapping. We consider that electrons in the $1S_e$ levels will increase the Auger rate as $k_{AR}N(N + 1)$, where N is the number of electrons in the $1S_e$ level, while the radiative rate increases as $k_{rad}(N + 1)$. If we assume there is also a constant rate of hole (or electron) trapping k_{tr}, then the PLQY is given by

$$\mathrm{PLQY} = \frac{k_{rad} \times (N + 1)}{k_{rad} \times (N + 1) + k_{AR} \times N \times (N + 1) + k_{tr}} \quad (1)$$

In eq 1, k_{rad} is the radiative recombination rate constant for uncharged QDs, $2k_{AR}$ is the AR rate constant for singly charged QDs (i.e., the trion decay constant), and k_{tr} is the trapping rate constant. With this simple model, we can reproduce the variation in PL intensity as a function of the number of electrons in the CB edge (N) reasonably well (Supporting Information, Figure S19) by inserting values for k_{rad}, k_{tr}, and k_{AR} from the literature [1/(30 ns), 1/(500 ps), and 1/(600 ps), respectively]. We note that eq 1 contains many simplifications. Most importantly, it assumes that all QDs are identical and can be occupied by a fractional number of electrons to mimic ensemble occupation. As such, it represents a qualitative approach to describing the photophysics in these charged QD films.

Equation 1 predicts that an increase in PLQY followed by a decrease upon charge injection is observed when $k_{tr} > k_{AR}$. However, if the opposite is true, then the PL will only drop upon increasing N and no PL maximum is observed. The latter is the case for thicker CdS shells ($x > 4$) and for the CdSe/CdS/ZnS samples, as can be seen in Figures 3f,h, S12−S14, S17, and S18. Because it is well known that k_{AR} decreases with increasing shell thickness,[14] this implies that k_{tr} decreases even more quickly with increasing shell thickness, or with the addition of a ZnS shell. This is in line with the increase in PLQY (Table S2).

When approximately two electrons are injected into the $1S_e$ levels, a second PL band is observed, which is typically assigned to radiative recombination involving electrons in the higher 1P-state in the CB and is also referred to in literature as negative tetron PL (Figures 3e,g and 4d).[30,63−65] We find that for thin CdS shells, there is negligible to no negative tetron luminescence (Figure 3c), even if the $1S_e$ level is almost completely filled (and the $1S_{3/2}1S_e$ transition almost entirely bleached, $\langle N_{1S_e} \rangle$ = 1.7, Figure S7) according to differential absorbance measurements (Figure 3d). This means that a part of the ensemble of the QD film has two electrons in the CB edge, and therefore that optical excitation should give rise to population of the $1P_e$ state in those QDs. When the shell thickness is increased, more apparent tetron PL is observed (Figures 3e and S9−S14). As shown in Figures 3g−h and S18, the CdSe/2CdS/ZnS and CdSe/6CdS/ZnS core/shell/shell QDs also display tetron PL. The fact that tetron PL is only observed for thicker CdS shells and ZnS shells might be related to the enhanced electrochemical stability of the core/shell(/shell) QDs and the associated higher charge densities that can be obtained.

CONCLUSIONS

In conclusion, by correlating in situ absorbance and PL SEC measurements, we find that shallow trap states near the CB edge, associated with the CdS surface, give rise to nonradiative recombination in CdSe/CdS QDs, even for shells as thick as 12 monolayers. These surface traps have a detrimental effect on the optoelectronic properties of colloidal core/shell QDs due to efficient hole trapping when the Fermi level is raised. We hypothesize that the traps originate on undercoordinated Cd surface atoms, potentially in the form of Cd−Cd dimers. These surface traps are removed by epitaxial growth of a wide band gap ZnS shell, which not only results in QDs with high PLQY values but also makes the PL intensity independent on the position of the Fermi level, as long as it is inside the band gap of the QDs. Furthermore, we find that the growth of wide band gap shells greatly enhances the electrochemical stability. Finally, we analyzed the radiative and nonradiative pathways as a function of the applied potential and show that, for thin CdS shells at relatively low doping densities, radiative recombination of negative trions dominates over nonradiative AR. When the doping density is increased (≫2 electrons in the CB edge), negative tetron and trion PL coincide within the ensemble, but the overall number of emitted photons is lower due to an increase in nonradiative AR pathways. Our results highlight the potential of SEC to analyze colloidal nanomaterials and elucidate the effect of shallow trap states on the photophysics of core/shell CdSe/CdS QDs.

DOI: 10.1021/acs.chemmater.9b02908
Chem. Mater. 2019, 31, 8484−8493

■ ASSOCIATED CONTENT

Supporting Information

The Supporting Information is available free of charge on the ACS Publications website at DOI: 10.1021/acs.chemmater.9b02908.

TEM images and electron diffraction patterns of core CdSe and core/shell CdSe/CdS QDs and CdSe/CdS/ZnS core/shell/shell QDs, PLQY, CV of ferrocene/ferrocenium calibration, differential absorbance plots for CdSe and CdSe/2CdS QDs, band offset determination core/shell CdSe/CdS QDs, validation of the band offset determination and global fit procedure, in situ PL SEC measurements on CdSe nanocrystals, in situ SEC measurements on CdSe/xCdS QDs (x = 2, 4, 6, 10, 12), CA measurements on CdSe/8CdS QD films at applied potential of −0.85 V and −1.5 V, in situ SEC measurements on CdSe/6CdS QDs prepared with a different synthesis protocol and CdSe/6CdS/ZnS nanocrystals, qualitative model for radiative and nonradiative recombination, and schematics of the spectroelectrochemical setups (PDF)

■ AUTHOR INFORMATION

Corresponding Authors

*E-mail: w.vanderstam@uu.nl (W.v.d.S.).
*E-mail: a.j.houtepen@tudelft.nl (A.J.H.).

ORCID

Ward van der Stam: 0000-0001-8155-5400
Gianluca Grimaldi: 0000-0002-2626-9118
Jaco J. Geuchies: 0000-0002-0758-9140
Solrun Gudjonsdottir: 0000-0002-4793-8747
Nicholas Kirkwood: 0000-0002-7845-7081
Arjan J. Houtepen: 0000-0001-8328-443X

Present Addresses

†Inorganic Chemistry and Catalysis, Debye Institute for Nanomaterials Science, Universiteitsweg 99, Utrecht University.
‡University of Melbourne, Chemistry, Parkville, Melbourne, VIC, AUS 3010.

Author Contributions

The manuscript was written through contributions of all the authors. All the authors have given approval to the final version of the manuscript.

Notes

The authors declare no competing financial interest.

■ ACKNOWLEDGMENTS

A.J.H. acknowledges support from the European Research Council Horizon 2020 ERC Grant agreement no. 678004 (Doping on Demand). The authors acknowledge Anneke Kraamer and Hamit Eren for valuable discussions.

■ REFERENCES

(1) Chen, O.; Zhao, J.; Chauhan, V. P.; Cui, J.; Wong, C.; Harris, D. K.; Wei, H.; Han, H.-S.; Fukumura, D.; Jain, R. K.; Bawendi, M. G. Compact High-Quality CdSe−CdS Core−Shell Nanocrystals with Narrow Emission Linewidths and Suppressed Blinking. *Nat. Mater.* **2013**, *12*, 445−451.

(2) de Mello Donega, C. Synthesis and Properties of Colloidal Heteronanocrystals. *Chem. Soc. Rev.* **2011**, *40*, 1512−1546.

(3) Justo, Y.; Goris, B.; Kamal, J. S.; Geiregat, P.; Bals, S.; Hens, Z. Multiple Dot-in-Rod PbS/CdS Heterostructures with High Photoluminescence Quantum Yield in the Near-Infrared. *J. Am. Chem. Soc.* **2012**, *134*, 5484−5487.

(4) Carbone, L.; Nobile, C.; De Giorgi, M.; Della Sala, F.; Morello, G.; Pompa, P.; Hytch, M.; Snoeck, E.; Fiore, A.; Franchini, I. R.; Nadasan, M.; Silvestre, A. F.; Chiodo, L.; Kudera, S.; Cingolani, R.; Krahne, R.; Manna, L. Synthesis and Micrometer-Scale Assembly of Colloidal CdSe/CdS Nanorods Prepared by a Seeded Growth Approach. *Nano Lett.* **2007**, *7*, 2942−2950.

(5) Xia, C.; Winckelmans, N.; Prins, P. T.; Bals, S.; Gerritsen, H. C.; de Mello Donega, C. Near-Infrared-Emitting $CuInS_2$/ZnS Dot-in-Rod Colloidal Heteronanorods by Seeded Growth. *J. Am. Chem. Soc.* **2018**, *140*, 5755−5763.

(6) Nakonechnyi, I.; Sluydts, M.; Justo, Y.; Jasieniak, J.; Hens, Z. Mechanistic Insights in Seeded Growth Synthesis of Colloidal Core/Shell Quantum Dots. *Chem. Mater.* **2017**, *29*, 4719−4727.

(7) Chen, Y.; Vela, J.; Htoon, H.; Casson, J. L.; Werder, D. J.; Bussian, D. A.; Klimov, V. I.; Hollingsworth, J. A. "Giant" Multishell CdSe Nanocrystal Quantum Dots with Suppressed Blinking. *J. Am. Chem. Soc.* **2008**, *130*, 5026−5027.

(8) van der Stam, W.; Bladt, E.; Rabouw, F. T.; Bals, S.; de Mello Donega, C. Near-Infrared Emitting $CuInSe_2$/$CuInS_2$ Dot Core/Rod Shell Heteronanorods by Sequential Cation Exchange. *ACS Nano* **2015**, *9*, 11430−11438.

(9) Groeneveld, E.; Witteman, L.; Lefferts, M.; Ke, X.; Bals, S.; Van Tendeloo, G.; de Mello Donega, C. Tailoring ZnSe-CdSe Colloidal Quantum Dots *via* Cation Exchange: From Core/Shell to Alloy Nanocrystals. *ACS Nano* **2013**, *7*, 7913−7930.

(10) Rabouw, F. T.; Vaxenburg, R.; Bakulin, A. A.; van Dijk-Moes, R. J. A.; Bakker, H. J.; Rodina, A.; Lifshitz, E.; Efros, A. L.; Koenderink, A. F.; Vanmaekelbergh, D. Dynamics of Intraband and Interband Auger Processes in Colloidal Core-Shell Quantum Dots. *ACS Nano* **2015**, *9*, 10366−10376.

(11) Rabouw, F. T.; Kamp, M.; van Dijk-Moes, R. J. A.; Gamelin, D. R.; Koenderink, A. F.; Meijerink, A.; Vanmaekelbergh, D. Delayed Exciton Emission and Its Relation to Blinking in CdSe Quantum Dots. *Nano Lett.* **2015**, *15*, 7718−7725.

(12) Nasilowski, M.; Spinicelli, P.; Patriarche, G.; Dubertret, B. Gradient CdSe/CdS Quantum Dots with Room Temperature Biexciton Unity Quantum Yield. *Nano Lett.* **2015**, *15*, 3953−3958.

(13) Rabouw, F. T.; Lunnemann, P.; van Dijk-Moes, R. J. A.; Frimmer, M.; Pietra, F.; Koenderink, A. F.; Vanmaekelbergh, D. Reduced Auger Recombination in Single CdSe/CdS Nanorods by One-Dimensional Electron Delocalization. *Nano Lett.* **2013**, *13*, 4884−4892.

(14) García-Santamaría, F.; Brovelli, S.; Viswanatha, R.; Hollingsworth, J. A.; Htoon, H.; Crooker, S. A.; Klimov, V. I. Breakdown of Volume Scaling in Auger Recombination in CdSe/CdS Heteronanocrystals: The Role of the Core-Shell Interface. *Nano Lett.* **2011**, *11*, 687−693.

(15) Park, Y.-S.; Lim, J.; Makarov, N. S.; Klimov, V. I. Effect of Interfacial Alloying versus "Volume Scaling" on Auger Recombination in Compositionally Graded Semiconductor Quantum Dots. *Nano Lett.* **2017**, *17*, 5607−5613.

(16) Park, Y.-S.; Malko, A. V.; Vela, J.; Chen, Y.; Ghosh, Y.; García-Santamaría, F.; Hollingsworth, J. A.; Klimov, V. I.; Htoon, H. Near-Unity Quantum Yields of Biexciton Emission from CdSe/CdSNanocrystals Measured Using Single-Particle Spectroscopy. *Phys. Rev. Lett.* **2011**, *106*, 187401.

(17) Coropceanu, I.; Rossinelli, A.; Caram, J. R.; Freyria, F. S.; Bawendi, M. G. Slow-Injection Growth of Seeded CdSe/CdS Nanorods with Unity Fluorescence Quantum Yield and Complete Shell to Core Energy Transfer. *ACS Nano* **2016**, *10*, 3295−3301.

(18) Pu, C.; Peng, X. To Battle Surface Traps on CdSe/CdS Core/Shell Nanocrystals: Shell Isolation *versus* Surface Treatment. *J. Am. Chem. Soc.* **2016**, *138*, 8134−8142.

(19) Pu, C.; Qin, H.; Gao, Y.; Zhou, J.; Wang, P.; Peng, X. Synthetic Control of Exciton Behavior in Colloidal Quantum Dots Synthetic

DOI: 10.1021/acs.chemmater.9b02908
Chem. Mater. 2019, 31, 8484−8493

Control of Exciton Behavior in Colloidal Quantum Dots. *J. Am. Chem. Soc.* **2017**, *139*, 3302−3311.
(20) Houtepen, A. J.; Hens, Z.; Owen, J. S.; Infante, I. On the Origin of Surface Traps in Colloidal II-VI Semiconductor Nanocrystals. *Chem. Mater.* **2017**, *29*, 752−761.
(21) Zhou, J.; Zhu, M.; Meng, R.; Qin, H.; Peng, X. Ideal CdSe/CdS Core/Shell Nanocrystals Enabled by Entropic Ligands and Their Core Size-, Shell Thickness-, and Ligand-Dependent Photoluminescence Properties. *J. Am. Chem. Soc.* **2017**, *139*, 16556−16567.
(22) Talapin, D. V.; Koeppe, R.; Götzinger, S.; Kornowski, A.; Lupton, J. M.; Rogach, A. L.; Benson, O.; Feldmann, J.; Weller, H. Highly Emissive Colloidal CdSe/CdS Heterostructures of Mixed Dimensionality. *Nano Lett.* **2003**, *3*, 1677−1681.
(23) Talapin, D. V.; Lee, J.-S.; Kovalenko, M. V.; Shevchenko, E. V. Prospects of Colloidal Nanocrystals for Electronic and Optoelectronic Applications. *Chem. Rev.* **2010**, *110*, 389−458.
(24) Shirasaki, Y.; Supran, G. J.; Bawendi, M. G.; Bulović, V. Emergence of Colloidal Quantum-Dot Light-Emitting Technologies. *Nat. Photonics* **2012**, *7*, 13−23.
(25) Pinchetti, V.; Meinardi, F.; Camellini, A.; Sirigu, G.; Christodoulou, S.; Bae, W. K.; De Donato, F.; Manna, L.; Zavelani-Rossi, M.; Moreels, I.; Klimov, V. I.; Brovelli, S. Effect of Core/Shell Interface on Carrier Dynamics and Optical Gain Properties of Dual-Color Emitting CdSe/CdS Nanocrystals. *ACS Nano* **2016**, *10*, 6877−6887.
(26) Brovelli, S.; Bae, W. K.; Galland, C.; Giovanella, U.; Meinardi, F.; Klimov, V. I. Dual-Color Electroluminescence from Dot-in-Bulk Nanocrystals. *Nano Lett.* **2014**, *14*, 486−494.
(27) le Feber, B.; Prins, F.; de Leo, E.; Rabouw, F. T.; Norris, D. J. Colloidal-Quantum-Dot Ring Lasers with Active Color Control. *Nano Lett.* **2018**, *18*, 1028−1034.
(28) Grim, J. Q.; Christodoulou, S.; Di Stasio, F.; Krahne, R.; Cingolani, R.; Manna, L.; Moreels, I. Continuous-Wave Biexciton Lasing at Room Temperature Using Solution-Processed Quantum Wells. *Nat. Nanotechnol.* **2014**, *9*, 891−895.
(29) Javaux, C.; Mahler, B.; Dubertret, B.; Shabaev, A.; Rodina, A. V.; Efros, A. L.; Yakovlev, D. R.; Liu, F.; Bayer, M.; Camps, G.; Biadala, L.; Buil, S.; Quelin, X.; Hermier, J.-P. Thermal Activation of Non-Radiative Auger Recombination in Charged Colloidal Nanocrystals. *Nat. Nanotechnol.* **2013**, *8*, 206−212.
(30) Jha, P. P.; Guyot-Sionnest, P. Photoluminescence Switching of Charged Quantum Dot Films. *J. Phys. Chem. C* **2007**, *111*, 15440−15445.
(31) Gooding, A. K.; Gómez, D. E.; Mulvaney, P. The Effects of Electron and Hole Injection on the Photoluminescence of CdSe/CdS/ZnS Nanocrystal Monolayers. *ACS Nano* **2008**, *2*, 669−676.
(32) du Fossé, I.; ten Brinck, S.; Infante, I.; Houtepen, A. J. The Role of Surface Reduction in the Formation of Traps in n-Doped II-VI Semiconductor Nanocrystals: How to Charge without Reducing the Surface. *Chem. Mater.* **2019**, *31*, 4575−4583.
(33) Qu, L.; Peng, Z. A.; Peng, X. Alternative Routes toward High Quality CdSe Nanocrystals. *Nano Lett.* **2001**, *1*, 333−337.
(34) Li, J. J.; Wang, Y. A.; Guo, W.; Keay, J. C.; Mishima, T. D.; Johnson, M. B.; Peng, X. Large-Scale Synthesis of Nearly Monodisperse CdSe/CdS Core/Shell Nanocrystals Using Air-Stable Reagents via Successive Ion Layer Adsorption and Reaction. *J. Am. Chem. Soc.* **2003**, *125*, 12567−12575.
(35) Jasieniak, J.; Smith, L.; van Embden, J.; Mulvaney, P.; Califano, M. Re-Examination of the Size-Dependent Absorption Properties of CdSe Quantum Dots. *J. Phys. Chem. C* **2009**, *113*, 19468−19474.
(36) Boldt, K.; Kirkwood, N.; Beane, G. A.; Mulvaney, P. Synthesis of Highly Luminescent and Photo-Stable, Graded Shell CdSe/$Cd_xZn_{1-x}S$ Nanoparticles by In Situ Alloying. *Chem. Mater.* **2013**, *25*, 4731−4738.
(37) Boehme, S. C.; Wang, H.; Siebbeles, L. D. A.; Vanmaekelbergh, D.; Houtepen, A. J. Electrochemical Charging of CdSe Quantum Dot Films: Dependence on Void Size and Counterion Proximity. *ACS Nano* **2013**, *7*, 2500−2508.
(38) Ruch, P. W.; Cericola, D.; Hahn, M.; Kötz, R.; Wokaun, A. On the Use of Activated Carbon as a Quasi-Reference Electrode in Non-Aqueous Electrolyte Solutions. *J. Electroanal. Chem.* **2009**, *636*, 128−131.
(39) van der Stam, W.; Gudjonsdottir, S.; Evers, W. H.; Houtepen, A. J. Switching between Plasmonic and Fluorescent Copper Sulfide Nanocrystals. *J. Am. Chem. Soc.* **2017**, *139*, 13208−13217.
(40) Brovelli, S.; Bae, W. K.; Meinardi, F.; Santiago González, B.; Lorenzon, M.; Galland, C.; Klimov, V. I. Electrochemical Control of Two-Color Emission from Colloidal Dot-in-Bulk Nanocrystals. *Nano Lett.* **2014**, *14*, 3855−3863.
(41) Chen, M.; Guyot-Sionnest, P. Reversible Electrochemistry of Mercury Chalcogenide Colloidal Quantum Dot Films. *ACS Nano* **2017**, *11*, 4165−4173.
(42) Zhai, Y.; Zhu, Z.; Zhou, S.; Zhu, C.; Dong, S. Recent Advances in Spectroelectrochemistry. *Nanoscale* **2018**, *10*, 3089−3111.
(43) Carroll, G. M.; Tsui, E. Y.; Brozek, C. K.; Gamelin, D. R. Spectroelectrochemical Measurement of Surface Electrostatic Contributions to Colloidal CdSe Nanocrystal Redox Potentials. *Chem. Mater.* **2016**, *28*, 7912−7918.
(44) Boehme, S. C.; Azpiroz, J. M.; Aulin, Y. V.; Grozema, F. C.; Vanmaekelbergh, D.; Siebbeles, L. D. A.; Infante, I.; Houtepen, A. J. Density of Trap States and Auger-Mediated Electron Trapping in CdTe Quantum-Dot Solids. *Nano Lett.* **2015**, *15*, 3056−3066.
(45) Shallcross, R. C.; Zheng, Y.; Saavedra, S. S.; Armstrong, N. R. Determining Band-Edge Energies and Morphology-Dependent Stability of Formamidinium Lead Perovskite Films Using Spectroelectrochemistry and Photoelectron Spectroscopy. *J. Am. Chem. Soc.* **2017**, *139*, 4866−4878.
(46) Gudjonsdottir, S.; van der Stam, W.; Kirkwood, N.; Evers, W. H.; Houtepen, A. J. The Role of Dopant Ions on Charge Injection and Transport in Electrochemically Doped Quantum Dot Films. *J. Am. Chem. Soc.* **2018**, *140*, 6582−6590.
(47) Alimoradi Jazi, M.; Janssen, V. A. E. C.; Evers, W. H.; Tadjine, A.; Delerue, C.; Siebbeles, L. D. A.; van der Zant, H. S. J.; Houtepen, A. J.; Vanmaekelbergh, D. Transport Properties of a Two-Dimensional PbSe Square Superstructure in an Electrolyte-Gated Transistor. *Nano Lett.* **2017**, *17*, 5238−5243.
(48) Noviandri, I.; Brown, K. N.; Fleming, D. S.; Gulyas, P. T.; Lay, P. A.; Masters, A. F.; Phillips, L. The Decamethylferrocenium/Decamethylferrocene Redox Couple: A Superior Redox Standard to the Ferrocenium/Ferrocene Redox Couple for Studying Solvent Effects on the Thermodynamics of Electron Transfer. *J. Phys. Chem. B* **1999**, *103*, 6713−6722.
(49) van der Stam, W.; de Graaf, M.; Gudjonsdottir, S.; Geuchies, J. J.; Dijkema, J. J.; Kirkwood, N.; Evers, W. H.; Longo, A.; Houtepen, A. J. Tuning and Probing the Distribution of Cu^+ and Cu^{2+} Trap States Responsible for Broad-Band Photoluminescence in $CuInS_2$ Nanocrystals. *ACS Nano* **2018**, *12*, 11244−11253.
(50) van der Stam, W.; du Fossé, I.; Grimaldi, G.; Monchen, J. O. V.; Kirkwood, N.; Houtepen, A. J. Spectroelectrochemical Signatures of Surface Trap Passivation on CdTe Nanocrystals. *Chem. Mater.* **2018**, *30*, 8052−8061.
(51) Frantsuzov, P. A.; Marcus, R. A. Explanation of Quantum Dot Blinking without the Long-Lived Trap Hypothesis. *Phys. Rev. B: Condens. Matter Mater. Phys.* **2005**, *72*, 155321.
(52) Califano, M.; Franceschetti, A.; Zunger, A. Temperature Dependence of Excitonic Radiative Decay in CdSe Quantum Dots: The Role of Surface Hole Traps. *Nano Lett.* **2005**, *5*, 2360−2364.
(53) Kirkwood, N.; Monchen, J. O. V.; Crisp, R. W.; Grimaldi, G.; Bergstein, H. A. C.; du Fossé, I.; van der Stam, W.; Infante, I.; Houtepen, A. J. Finding and Fixing Traps in II-VI and III-V Colloidal Quantum Dots: The Importance of Z-Type Ligand Passivation. *J. Am. Chem. Soc.* **2018**, *140*, 15712−15723.
(54) Park, S.; Barber, M. E. Thermodynamic Stabilities of Semiconductor Electrodes. *J. Electroanal. Chem.* **1979**, *99*, 67−76.
(55) Chen, S.; Wang, L.-W. Thermodynamic Oxidation and Reduction Potentials of Photocatalytic Semiconductors in Aqueous Solution. *Chem. Mater.* **2012**, *24*, 3659−3666.

DOI: 10.1021/acs.chemmater.9b02908
Chem. Mater. 2019, 31, 8484−8493

(56) Hughes, K. E.; Hartstein, K. H.; Gamelin, D. R. Photodoping and Transient Spectroscopies of Copper-Doped CdSe/CdS Nanocrystals. *ACS Nano* **2018**, *12*, 718−728.
(57) Cohn, A. W.; Rinehart, J. D.; Schimpf, A. M.; Weaver, A. L.; Gamelin, D. R. Size Dependence of Negative Trion Auger Recombination in Photodoped CdSe Nanocrystals. *Nano Lett.* **2014**, *14*, 353−358.
(58) Cohn, A. W.; Schimpf, A. M.; Gunthardt, C. E.; Gamelin, D. R. Size-Dependent Trap-Assisted Auger Recombination in Semiconductor Nanocrystals. *Nano Lett.* **2013**, *13*, 1810−1815.
(59) Hanifi, D. A.; Bronstein, N. D.; Koscher, B. A.; Nett, Z.; Swabeck, J. K.; Takano, K.; Schwartzberg, A. M.; Maserati, L.; Vandewal, K.; van de Burgt, Y.; Salleo, A.; Alivisatos, A. P. Redefining Near-Unity Luminescence in Quantum Dots with Photothermal Threshold Quantum Yield. *Science* **2019**, *363*, 1199−1202.
(60) Voznyy, O.; Thon, S. M.; Ip, A. H.; Sargent, E. H. Dynamic Trap Formation and Elimination in Colloidal Quantum Dots. *J. Phys. Chem. Lett.* **2013**, *4*, 987−992.
(61) Gilmore, R. H.; Liu, Y.; Shcherbakov-Wu, W.; Dahod, N. S.; Lee, E. M. Y.; Weidman, M. C.; Li, H.; Jean, J.; Bulović, V.; Willard, A. P.; Grossman, J. C.; Tisdale, W. A. Epitaxial Dimers and Auger-Assisted Detrapping in PbS Quantum Dot Solids. *Matter* **2019**, *1*, 250−265.
(62) Bard, A. J.; Faulkner, L. R. *Electrochemical Methods: Fundamentals and Applications*, 2nd ed.; John Wiley & Sons: Hoboken, NJ, 2000.
(63) Wang, C.; Wehrenberg, B. L.; Woo, C. Y.; Guyot-Sionnest, P. Light Emission and Amplification in Charged CdSe Quantum Dots. *J. Phys. Chem. B* **2004**, *108*, 9027−9031.
(64) Hartstein, K. H.; Erickson, C. S.; Tsui, E. Y.; Marchioro, A.; Gamelin, D. R. Electron Stability and Negative-Tetron Luminescence in Free-Standing Colloidal n-Type CdSe/CdS Quantum Dots. *ACS Nano* **2017**, *11*, 10430−10438.
(65) Shim, M.; Guyot-Sionnest, P. n-Type Colloidal Semiconductor Nanocrystals. *Nature* **2000**, *407*, 981−983.

DOI: 10.1021/acs.chemmater.9b02908
Chem. Mater. 2019, 31, 8484−8493